

Methane Activation by Platinum: Critical Role of Edge and Corner Sites of Metal Nanoparticles

Francesc Viñes,^{*,[a]} Yaroslava Lykhach,^[b] Thorsten Staudt,^[b] Michael P. A. Lorenz,^[b]
Christian Papp,^[b] Hans-Peter Steinrück,^[b, c] Jörg Libuda,^[b, c]
Konstantin M. Neyman,^[d, e] and Andreas Görling^[a]

Abstract: Complete dehydrogenation of methane is studied on model Pt catalysts by means of state-of-the-art DFT methods and by a combination of supersonic molecular beams with high-resolution photoelectron spectroscopy. The DFT results predict that intermediate species like CH₃ and CH₂ are specially stabilized at sites located at particles edges and corners by an amount of 50–80 kJ mol⁻¹. This stabilization is caused by an enhanced activity of low-coordinated sites accompanied by their special flexibility to accommodate adsorbates. The kinetics of the complete dehydrogenation of methane is sub-

stantially modified according to the reaction energy profiles when switching from Pt(111) extended surfaces to Pt nanoparticles. The CH₃ and CH₂ formation steps are endothermic on Pt(111) but markedly exothermic on Pt₇₉. An important decrease of the reaction barriers is observed in the latter case with values of approximately 60 kJ mol⁻¹ for first C–H bond scission

and 40 kJ mol⁻¹ for methyl decomposition. DFT predictions are experimentally confirmed by methane decomposition on Pt nanoparticles supported on an ordered CeO₂ film on Cu(111). It is shown that CH₃ generated on the Pt nanoparticles undergoes spontaneous dehydrogenation at 100 K. This is in sharp contrast to previous results on Pt single-crystal surfaces in which CH₃ was stable up to much higher temperatures. This result underlines the critical role of particle edge sites in methane activation and dehydrogenation.

Keywords: density functional calculations · methane activation · photoelectron spectroscopy · platinum · supersonic molecular beams

Introduction

Methane is the simplest, most abundant, and stable alkane molecule. In addition, it is the second most important anthropogenic greenhouse gas after CO₂.^[1] Its rise in air con-

centration is the result of non-sustainable farming, and chemical and energy power processes. Although the amount of methane emissions is five times less than those of CO₂, they are similarly problematic because methane can retain approximately 23 times more heat than CO₂ in the atmos-


[a] Dr. F. Viñes, Prof. Dr. A. Görling
Friedrich-Alexander-Universität Erlangen-Nürnberg
Lehrstuhl für Theoretische Chemie and Interdisciplinary Center
for Interface Controlled Processes
Egerlandstr. 3, 91058 Erlangen (Germany)
Fax: (+49)9131-85-27736
E-mail: Francesc.Vines@chemie.uni-erlangen.de

[b] Dr. Y. Lykhach, T. Staudt, Dr. M. P. A. Lorenz, Dr. C. Papp,
Prof. Dr. H.-P. Steinrück, Prof. Dr. J. Libuda
Friedrich-Alexander-Universität Erlangen-Nürnberg
Lehrstuhl für Physikalische Chemie II
Egerlandstr. 3, 91058 Erlangen (Germany)

[c] Prof. Dr. H.-P. Steinrück, Prof. Dr. J. Libuda
Erlangen Catalysis Resource Center
Friedrich-Alexander-Universität Erlangen-Nürnberg
91058 Erlangen (Germany)

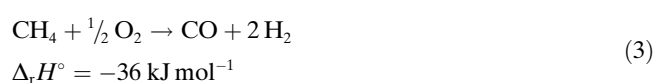
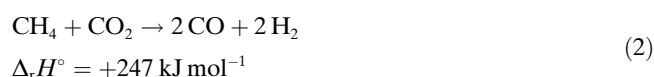
[d] Prof. Dr. K. M. Neyman
Departament de Química Física and
Institut de Química Teòrica i Computacional (IQTCUB)
Universitat de Barcelona, C/Martí i Franquès 1
08028 Barcelona (Spain)

[e] Prof. Dr. K. M. Neyman
Institució Catalana de Recerca i Estudis Avançats (ICREA)
08010 Barcelona (Spain)

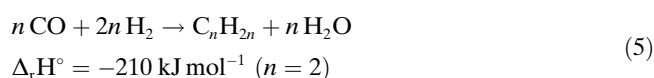
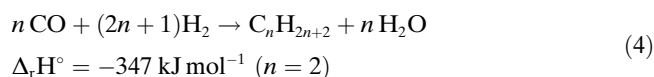
 Supporting information for this article is available on the WWW under <http://dx.doi.org/10.1002/chem.201000296>.

phere. Because of this, a large-scale chemical conversion of methane into other valuable and/or environmentally friendly chemical compounds would have a tremendous impact on the climate and, due to the low-cost of this feedstock, on the chemical industry.

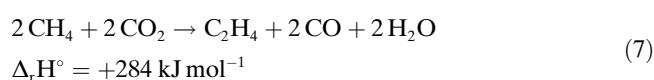
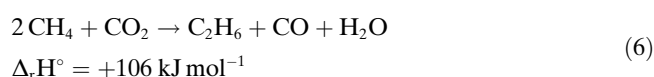
Once methane is activated, it can be used in a variety of industrially relevant reactions, for instance, synthesis-gas (syngas) formation,^[2,3] which can be achieved either through steam reforming [Eq. (1)],^[4-6] dry reforming [Eq. (2)],^[7-12] or methane partial oxidation [Eq. (3)].^[13-16]



The syngas H_2/CO current generated can be used in Fischer-Tropsch reaction^[4,17-20] to obtain long-chain hydrocarbons [Eqs. (4) and (5)]. In addition, the generation of H_2 could be relevant for usage in fuel cells.^[21-23]



Alternatively, methane can potentially be converted to ethane [Eq. (6)] and ethylene [Eq. (7)] through CO_2 oxidative coupling.^[24-27]



In spite of the broad range of potential applications, it is primarily the extraordinary chemical stability of methane that makes its activation, in particular the scission of the C–H bond, a serious challenge. Therefore, the catalytic activation of methane on transition metals has been a matter of intense investigation.^[28-30] Nickel is commonly used as a catalyst in many of the above-mentioned chemical reactions, either exposing extended surfaces^[4,24,31,32,35] or as supported nanoparticles.^[2,3,8,14,21,25] Theoretical^[33,34] and experimental^[32,35] studies on single-crystal surfaces indicate that the use of platinum instead of nickel catalysts could substantially reduce the energy barrier for the first hydrogen abstraction from methane, which is normally considered the reaction rate-limiting step.^[3] On Pt(111) surfaces the reduction in the activation barrier with respect to Ni(111) is around

15–30 kJ mol^{-1} . A similar reduction in activation enthalpy would apply for methyl dehydrogenation according to DFT calculations.^[36]

Herein, we provide theoretical and experimental evidence that usage of Pt nanoparticles instead of extended Pt surfaces dramatically facilitates the kinetics of methane dehydrogenation. The reason for the notable change in the reaction behavior is the presence of low-coordinated sites, such as edge, corner, and nearby sites on nanoparticles. The role of these sites is to reduce the energy barriers of every reaction step and to stabilize the reaction intermediates. In this sense, the use of platinum nanoparticles could make the formation of intermediates, such as CH species, an energetically downhill process that works at low temperatures. This pathway would therefore be preferred over the high-barrier energy-demanding process on extended Pt(111) surfaces. Past studies employing either slab^[37-39] or small cluster^[40-42] models have focused exclusively on low Miller index surfaces. The present work is among the first that comparatively analyzes the surface reactivity of extended transition-metal terraces and nanoparticles at the same high computational level, and includes subsequent experimental corroboration.

Experimental and Computational Details

Computational details and models: DFT calculations with periodic boundary conditions were carried out by using the program package VASP.^[43] Interactions of valence electrons with the atomic cores were described by the projector augmented wave method.^[44] A kinetic energy cutoff of 415 eV for the plane-wave basis set was employed throughout, ensuring convergence of energies to better than 0.01 kJ mol^{-1} . Geometry optimizations were performed using a conjugate gradient algorithm until forces acting on each atom became less than 0.03 $\text{kJ mol}^{-1}\text{pm}^{-1}$. Tests revealed no effect of spin polarization on the adsorbed systems. Thus, all calculations were non-spin polarized, unless stated otherwise. The revised form of the PBE^[45] (RPBE) exchange-correlation (xc) functional has been used throughout, as it has been shown to give accurate results for the adsorption of small molecules.^[45,46]

The transition states (TS) have been located by using the climbing-image nudged-elastic-band (CI-NEB) method connecting reactants and products adsorbed in the most stable positions. Structures near the TS have been refined by a quasi-Newton method until forces are less than 0.03 $\text{kJ mol}^{-1}\text{pm}^{-1}$. The proper character of the local minima and the TS have been confirmed by analysis of the vibrational frequencies of the adsorbed species through construction and diagonalization of the Hessian matrix applying displacements of 5 pm in each cell direction for each atom of the adsorbed species.

We have defined the calculated adsorption energy E_{ads} of a given species A on a Pt substrate B [nanoparticle or (111) surface] as shown in Equation (8):

$$E_{\text{ads}} = E_{\text{A/B}} - (E_{\text{A}} + E_{\text{B}}) \quad (8)$$

in which $E_{\text{A/B}}$ is the total energy of the adsorption system, E_{A} is the total energy of the isolated species A, and E_{B} is the total energy of the relaxed Pt substrate. According to this definition, negative energy values correspond to an energetically favorable adsorption. The reference energies E_{A} of the isolated species have been obtained by placing the species in the middle of a broken-symmetry unit cell of dimensions $9 \times 10 \times 11 \text{ \AA}$ and performing spin-polarized calculations in the case of open-shell species.

Reaction energy profiles for complete methane dehydrogenation have been constructed by assigning energetic positions (E_{rel}) of intermediate states, relative to a reference, defined by the sum of the total energies of gas-phase methane and the pristine relaxed substrate. The energy of each dissociation reactant, intermediate, or CH_x product ($x=0-4$) is calculated by the addition to the reference value of the energy required to form, from methane in the gas phase, this intermediate set [$\text{CH}_x + (4-x)\text{H}$] and the adsorption energies of the latter. That is, the relative energy of products of the first methane dehydrogenation step on Pt(111), $E_{\text{rel}}[(\text{CH}_3+\text{H})/\text{Pt}(111)]$, is obtained by the addition of the dissociation energy (ΔE_{diss}) of CH_4 to $\text{CH}_3 + \text{H}$ in the gas phase, $\Delta E_{\text{diss}} = E_{\text{CH}_3}(\text{g}) + E_{\text{H}}(\text{g}) - E_{\text{CH}_4}(\text{g})$, and the corresponding adsorption energies: $E_{\text{rel}}[(\text{CH}_3+\text{H})/\text{Pt}(111)] = E_{\text{CH}_3}(\text{g}) + E_{\text{H}}(\text{g}) - E_{\text{CH}_4}(\text{g}) + E_{\text{ads}}^{\text{Pt}(111)}(\text{CH}_3) + E_{\text{ads}}^{\text{Pt}(111)}(\text{H})$. Accordingly, the TS energies in the reaction profile are calculated by adding the energy difference between the TS and the corresponding initial state to the energy of the former, as specified above.

A correction has been applied throughout for the vibrational zero-point energy (ZPE) of the adsorbed species, except for the mode with the imaginary frequency at a TS. This means that for each vibrational mode, i , its ground state offset energy E_i defined by Equation (9) in which ν_i is the harmonic frequency of the mode i and h is the Planck constant, has been added to each energy profile value.

$$E_i = \frac{1}{2}h\nu_i \quad (9)$$

Due to the prohibitive computational costs, it is presently impossible to investigate the chemical behavior of nanoparticles greater than 1–2 nm in size by DFT calculations. Thus, a combined calculation strategy has been applied to study bigger nanoparticles (Figure 1) that has proven to provide a complete description in the past.^[46–48] This strategy consists of using two complementary models; the first is a reference six-layer (3×3) Pt(111) slab model to describe the chemical activity and reactivity of extended terraces and the inner regions of Pt nanoparticle facets, which usually exhibit to a large degree the most stable (111) surface, corresponding to a face-centered cubic (fcc) stacking. A Γ -centered \mathbf{k} -point grid of dimensions $6 \times 6 \times 1$ has been used for the slab model. Denser \mathbf{k} -point meshes lead to changes in energies below 1 kJ mol^{-1} . The second model is a cuboctahedral Pt_{79} nanoparticle exhibiting large (111) and small (100) facets. Metal nanoparticles of approximately 80 atoms have been shown to provide essentially size-converged results for the adsorption properties of species on them,^[49] and to be representative for the interaction between much larger nanoparticles.^[50] Moreover, properties such as average cohesion energies and average metal–metal bond lengths exhibit scalability with respect to particle size up to the bulk limit.^[51,52]

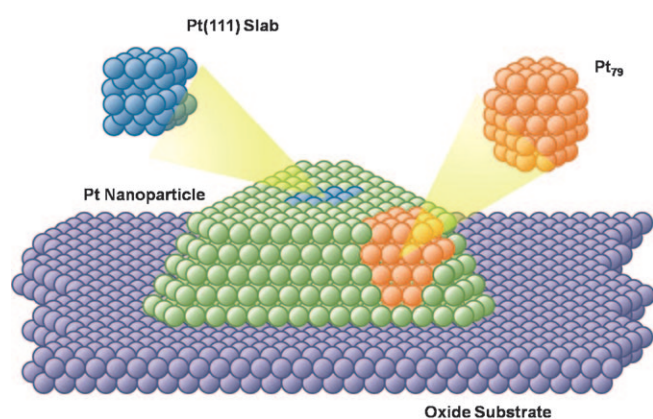


Figure 1. Sketch of a platinum nanoparticle of around 3.5 nm (green circles) supported on an oxide (violet circles). The Pt nanoparticle typically exhibiting large (111) facets and small (100) facets would be considered as a combination of a Pt(111) slab of six layers (blue circles) for description of the inner (111) facets, and Pt_{79} nanoparticles for modeling the edge, corner, and nearby sites.

Due to the large supercell size employed for such nanoparticles, converged results are obtained with calculations at one (Γ) \mathbf{k} -point. These nanoparticles can ideally complement the slab models, enabling the study of interactions of molecular species with defect sites like edges, corners, and sites nearby, which are present in significant number on supported metal catalysts and often are responsible for their special catalytic activity. Further computational details on both models, Pt(111) slabs as well as Pt_{79} clusters, can be found in a previous study.^[46] It is of note, however, that boundary sites that are in contact with the oxide support have not been taken into account.

Experimental: High-resolution photoelectron spectroscopy (HR-PES) studies on methane activation over the supported Pt nanoparticles were performed in a portable ultra-high vacuum (UHV) system, which was temporarily operated at the U49/2-PGM1 beamline at the synchrotron radiation facility BESSY II (Berlin). The samples were prepared by the deposition of a Pt layer with a nominal thickness of 0.5 nm onto a well-ordered 2.5 nm thick $\text{CeO}_2(111)/\text{Cu}(111)$ film at 300 K. Details of the sample preparation and treatment procedure can be found in the literature.^[53–55] The Pt/ $\text{CeO}_2/\text{Cu}(111)$ samples were exposed to a collimated supersonic molecular beam (SSMB) of CH_4 at a sample temperature of 100 K. The SSMB was generated from a resistively heated 100 μm molybdenum nozzle at a seeding ratio of 1:10 in a He environment. Previously, the kinetic energy (KE) of CH_4 was determined to be 68 kJ mol^{-1} (0.71 eV) under the conditions applied. The effective total pressure of the CH_4/He gas at the surface of the sample is 10^{-6} torr. The reaction products on the sample surface were observed in situ by positioning the sample at the intersection of the SSMB and the focal plane of the analyzer. In this geometry, the incidence angle of the SSMB is 0° with respect to the sample normal (normal incidence) and the detection angle for the photoelectrons is 45° . The C 1s core level spectra were acquired at a photon energy of 380 eV. With the analyzer operating at a constant pass energy of 10 eV, a total spectral resolution of 300 meV was achieved. The spectra were recorded in situ during exposure to the SSMB. To minimize irradiation-induced damage to the adsorbate layer, the synchrotron light was blocked by a shutter, which was opened only during acquisition of the spectra. The shutter opening time was 5 s per C 1s spectrum acquired.

Data analysis was based on previous experiments on Pt(111) performed under similar experimental conditions.^[56] The C 1s spectra were fitted with asymmetric Voigt profiles assuming that several CH_x species may coexist. Specifically, the peaks associated with CH_3 and CH were fitted with two components each, which accounted for the vibrational splitting. In particular, the energy difference between the adiabatic and the first vibrationally excited component was chosen as 0.40 eV for CH_3 and 0.42 eV for CH, with intensity ratios of 0.5 and 0.16, respectively. These values correspond to those observed for Pt(111).^[56] All peaks widths were kept constant for the fitted components.

Results and Discussion

Reactive species on Pt: DFT calculations: To create an energy profile of the complete methane dehydrogenation process, the adsorption of all involved species has been investigated on both a Pt(111) slab and on Pt_{79} nanoparticle models. The adsorbed species comprise CH_x species ($x=0-4$) and atomic hydrogen. All possible adsorption sites and coordination modes have been systematically investigated. The most stable adsorption sites for each species are depicted in Figure 2 together with their adsorption energies. It is of interest to note that no adsorption has been found for CH_4 on Pt(111), since the interactions with the substrate are mainly due to dispersive forces and thus not described at the present level of DFT. In this sense, methane can be

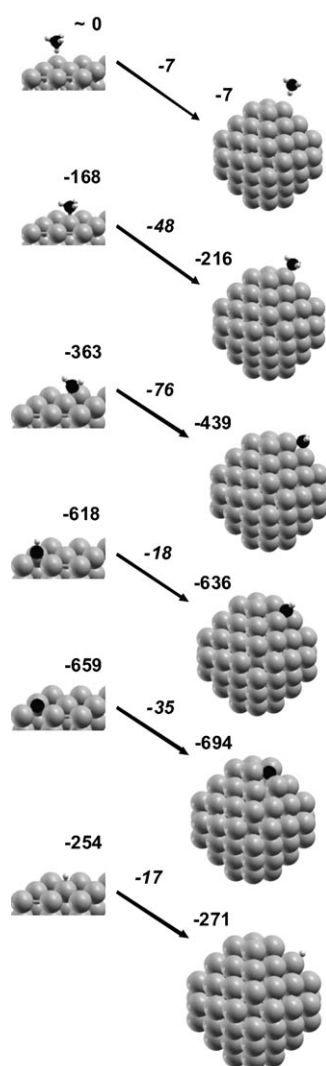


Figure 2. Most stable adsorption sites of CH_x and H species on Pt_{79} nanoparticle (right) and $\text{Pt}(111)$ slab (left). Bottom to top: H on on-top sites, C on fcc sites, CH on fcc sites, CH_2 on bridge sites, CH_3 on on-top sites, and CH_4 over slab and on top of a corner Pt atom of the nanoparticle. Values above the images are the adsorption energies (E_{ads}), whereas those above the arrows are difference in E_{ads} values between Pt_{79} and $\text{Pt}(111)$. All values are in kJ mol^{-1} . Large gray, black, and small gray spheres represent Pt, C, and H atoms, respectively.

thought of as a molecule rolling over the Pt substrates, which, according to literature, is only weakly bound to the surface by about 25 kJ mol^{-1} .^[57] On Pt_{79} , a very weak adsorption energy has been calculated for methane adsorbing in an on-top position at a corner site.

As far as preferable adsorption sites of involved CH_x and H species on $\text{Pt}(111)$ surfaces are concerned, present data agree with earlier theoretical results.^[37,38] Methyl (CH_3) prefers to adsorb on-top of a Pt atom, whereas methylene (CH_2) bridges two surface Pt atoms. Both methylidyne (CH) and carbon atoms prefer to be located over fcc three-fold hollow sites. Adsorption of CH and C on hexagonally cubic packed (hcp) sites is less stable by 10 and 15 kJ mol^{-1} , respectively, mainly due to steric repulsions with the Pt atom

located underneath the adsorption site in the second Pt layer.^[46] Moreover, the trend in the adsorption strengths is also consistent with previous slab model studies.^[37,38] Furthermore, the present slab models do not introduce the size-dependence problem of the earlier small cluster models, which may lead to oscillations in adsorption energies for a given site in the range of $20\text{--}80 \text{ kJ mol}^{-1}$. This can result in an adsorption energy for CH of more than 50 kJ mol^{-1} lower than that of isolated C atoms.^[40–42,58] Current adsorption energy values on $\text{Pt}(111)$ are $20\text{--}30 \text{ kJ mol}^{-1}$, smaller in comparison with past DFT studies^[37,38] using the Perdew–Wang 91 (PW91) xc functional,^[59] which is known to slightly overestimate the interaction between atoms. On the other hand, the RPBE functional often provides more accurate adsorption energies^[45] and, in fact, the present adsorption energy of atomic H, 254 kJ mol^{-1} , fits the experimental value of 256 kJ mol^{-1} .^[60] Present and past DFT calculations agree that atomic hydrogen on $\text{Pt}(111)$ can easily occupy different surface sites, such as bridge and hollow sites, on which it is only 4 kJ mol^{-1} more weakly adsorbed than on the most strongly binding on-top site.

In general, RPBE values by Ford et al.^[38] reveal a good agreement with our findings on $\text{Pt}(111)$, although present values for the adsorption energies of CH and C are lower by approximately 50 kJ mol^{-1} . This, however, could find an explanation in the following facts. Ford et al. carried out RPBE calculations at a surface coverage of $1/4$ monolayers (ML), whereas the present calculations were performed at the lower coverage of $1/9$ ML. The lower the coverage, the lesser the possible repulsions between adsorbates and the stronger the interaction with the substrate. Since CH and C become substantially negatively charged upon adsorption—the values according to a topological Bader charge analysis^[61] are -0.31 and -0.49 e , respectively—a significant lateral repulsion is expected for these species. In contrast, such a repulsion is not present for the other species, which remain almost neutral upon adsorption.

Species formed during methane decomposition adopt on the Pt_{79} cuboctahedral nanoparticle the same coordination modes as on $\text{Pt}(111)$, although they always involve corner (CH_4 , CH_3 , C), edge (H), or both corner and edge Pt atoms (CH_2 , CH). The main result here is that, in all cases, an adsorption stabilization occurs (see Figure 2). In fact, the lower coordination of Pt atoms located at defect sites, such as edges and corners, not only makes them more active to bind adsorbates, but they are, in addition, more flexible to accommodate species on them. This structural flexibility of Pt_{79} seems to be particularly important for the accommodation of C atoms. Here, the Pt–Pt bonds are elongated by 50 pm , which is 30 pm more than the bonds in $\text{Pt}(111)$. The flexibility effect is notably reduced for the rest of the species, with Pt–Pt distances elongation/contraction up to 13 pm , which, on Pt_{79} , is more pronounced by $2\text{--}4 \text{ pm}$ than on the $\text{Pt}(111)$ slab. This combination of factors is translated into the stabilization energy values, which can be quite significant for molecules such as CH_4 , CH_3 , and CH_2 in which the effect of edge and corner sites represents an increase of

more than 20% in the adsorption energy. For other species such as CH, C, and H, the effect is rather mild, that is below 7%, of the adsorption energy. Current results agree with experimental results of Papp et al.,^[62] who found after methane dissociation on a Pt(355) single crystal a higher methyl coverage at steps of the Pt(355) surface than on terraces locally featuring a (111) structure. DFT results on a Pd₇₉ cluster also showed much stronger stabilization at nanoparticle edges for CH₃ and CH₂, 23 and 27 kJ mol⁻¹, respectively, and a weaker stabilization of CH and C, 15 and 6 kJ mol⁻¹.^[63] Moreover, the present results are also in line with previous DFT studies^[39] on a reconstructed Pt(110) surface, where CH_x species are somewhat stronger bound near low-coordinated Pt atoms located at surface ridges. Nevertheless, the effect is much less important on Pt(110), with stabilization energies smaller by roughly a factor of two.

Dehydrogenation steps of CH₄ on Pt: DFT calculations:

The energy barriers for the sequential CH_x dehydrogenation reaction steps taking place either on the extended Pt(111) surface or on the Pt₇₉ nanoparticle have been obtained (Figure 3). Two approximations were made to construct the reaction profile depicted in this figure. First, from the substantial number of potential pathways with different initial and final configurations for each reaction step, only the particular pathway was calculated that connects the reaction species adsorbed on the most-stable sites. This seems justified since a recent systematic exploration of the pathway for first methane C–H scission on Pt(111) and Ni(111) slabs^[33] showed variations of the energy barriers below 5 kJ mol⁻¹.

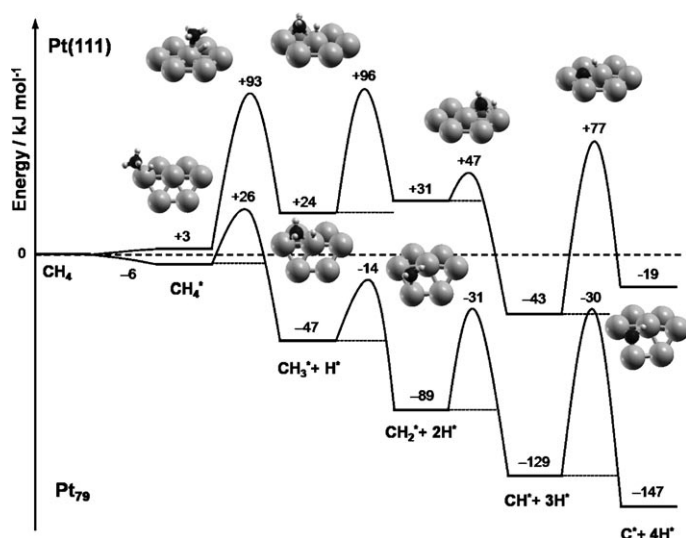


Figure 3. ZPE-corrected reaction energy profile for the complete dehydrogenation of methane on a Pt(111) surface and on a Pt₇₉ nanoparticle. All energies, in kJ mol⁻¹, refer to methane in the gas phase and the clean substrate. In the sketches of the transition states, only small portions containing seven Pt atoms of the calculated slab and cluster models are displayed for the sake of visual recognition. See the Computational Details section for further information about the construction of the reaction energy profile.

Second, it is assumed that after each reaction step, the hydrogen atoms may diffuse over the substrate to reach adsorption sites where no steric repulsion is present between H atoms and the remaining CH_x species, or between the H atoms themselves. This approximation is supported by an almost negligible diffusion barrier for H, with experimental estimates below 10 kJ mol⁻¹^[64] and theoretical calculations yielding even lower values (below 4 kJ mol⁻¹ according to the present and previous^[38] DFT data). Further tests for selected systems showed repulsion between CH_x and H to be smaller than 4 kJ mol⁻¹.

The calculated, non-ZPE-corrected activation barrier for the first C–H bond scission of methane, 102 kJ mol⁻¹, is somewhat larger than the experimental values of (75 ± 3) kJ mol⁻¹.^[65–67] The ZPE correction reduces the energy barrier to 90 kJ mol⁻¹, thus in fair agreement with the experimental value. Besides, limitations in the accuracy of DFT functionals could explain most of the remaining difference.^[68] DFT calculations using small planar clusters showed activation barriers of the same order of magnitude,^[40,69,70] although variations with respect to present data of 15–30 kJ mol⁻¹ are found, depending on the cluster size and the xc functional employed. A more direct comparison can be made to other DFT studies employing periodic boundary conditions; Michaelides and Hu^[71] summarized complete methane dehydrogenation on Pt(111) calculated at the PW91 level employing a fixed three-layered slab. Nave and Jackson^[33] calculated the first dehydrogenation step of methane with the PBE xc functional^[72] over a fixed four-layered slab displaying experimental Pt–Pt distances. In the case of the first hydrogen abstraction energy barrier, our non-ZPE-corrected value is in line with the estimated barrier of Nave and Jackson of 90 kJ mol⁻¹.^[33] The disagreement with the value reported of Michaelides and Hu of 65 kJ mol⁻¹ seems to arise from the exothermicity of the reaction step rather than from the transition state itself.^[71] Indeed, the authors found that abstraction of the first H atom in methane is exothermic by 8 kJ mol⁻¹. Present and earlier results show that this step is endothermic by 16–25 kJ mol⁻¹. Perfect agreement is reached when the endothermicity value is adjusted to the work of Michaelides and Hu.^[71]

ZPE-corrected energy profiles for methane dehydrogenation over both the Pt(111) slab and Pt₇₉ nanoparticle are depicted in Figure 3. Focusing first on Pt(111), the initial dehydrogenation barrier can be overcome experimentally in a direct dissociation process using an SSMB with sufficient KE. After activation, the internal and kinetic energies are efficiently dissipated, leading to the kinetic stabilization of methyl species at low temperatures. Evolution to methylene, or the reverse reaction to form methane, would require relatively high energy barriers of approximately 70 kJ mol⁻¹ to be overcome. At sufficiently high temperature (and coverage) this may be possible, leading to formation of methane and methylene. The latter, however, would rapidly undergo further dehydrogenation to eventually form the most-stable species on a Pt(111) surface, methylidyne. This is in excellent agreement with experimental results of Fuhrmann

et al.,^[56] who detected methyl species on Pt(111) single crystals at low temperature and found that, upon heating to 260 K, methyl simultaneously recombines to form methane and decomposes to form methylidyne. Once methylidyne is formed, the system is trapped in a thermodynamic sink. The reverse reaction to methane is unlikely since recombination and desorption of hydrogen would be preferred. According to our calculations, the reaction of adsorbed hydrogen atoms to form gas phase H_2 is endothermic by only 67 kJ mol^{-1} . In this sense, H_2 (g) would disappear while methylidyne is formed. The only possible subsequent reaction step at low hydrogen pressure is the formation of surface carbon, which is reported to occur at temperatures above 500 K.^[56] The value is in line with the high value of 120 kJ mol^{-1} for the calculated energy barrier. At sufficiently high coverage, carbon atoms would gather to form monolayer graphene,^[46] which has been detected when heating above 890 K.^[73]

What happens when methane dehydrogenates on Pt nanoparticles instead of extended surfaces? The role of defect sites, such as edge and corner sites, is clearly visible in the reaction profile of the Pt_{79} nanoparticle in Figure 3. As introduced in the previous section, the stabilization of reaction intermediate species at particles edges/corners completely changes the reaction profile from slightly exothermic, or isoenergetic for formation of atomic carbon on Pt(111), to a clearly exothermic process on Pt_{79} . Moreover, ZPE corrections ultimately lead to a change of the thermodynamic sink, with atomic C becoming the most stable species on the nanoparticle (see Figure S1 in the Supporting Information). This finding suggests that C formation is accelerated when using Pt nanoparticles. As far as the kinetic aspects are concerned, all the energy barriers are reduced when compared with those on Pt(111) for the same reaction steps. This effect is most pronounced for methyl and methylene formation. Here the barriers drop substantially when using nanoparticles to values that are roughly $2/3$ of those on Pt(111) extended surfaces. The most important finding, however, is that, with the exception of methylidyne dehydrogenation to carbon, the heights of the barriers appear to be governed by the relative positions of reactants and products. In this sense, the difference between the reaction barriers for the first dehydrogenation step from CH_4 to $CH_3 + H$ (58 kJ mol^{-1}) is very similar to the difference of reaction energies (62 kJ mol^{-1}) on Pt_{79} and Pt(111). The same behavior is observed for the methylene and methylidyne formation steps, within an accuracy of 10 kJ mol^{-1} .

Since this is the first DFT study of complete methane dehydrogenation on metal nanoparticles, no comparison with previous data is possible. To date, the most similar system studied by DFT methods is the Pt(110) reconstructed surface.^[39] In this case, every second row of Pt surface atoms is removed, thus generating a corrugated surface containing grooves and ridges. In fact, the stabilization of CH_x species in the vicinity of the low-coordinated Pt ridges^[39] leads to a reaction profile that resembles the non-ZPE energy profile on Pt_{79} (see Figure S1 in the Supporting Information).

In summary, the thermodynamic energy profile and reaction energy barriers found on Pt_{79} strongly suggest more facile methane activation and complete dehydrogenation relative to Pt(111). Methyl formation should be feasible by employing lower kinetic energies than on Pt(111), and once formed the species would undergo rapid decomposition to follow the downhill route to methylidyne. DFT calculations explain why, on stepped Pt surfaces,^[62] methyl dehydrogenation occurs in the 160–220 K temperature range, which is noticeably lower than on Pt(111). Once methylidyne is formed, the back reaction to methane on nanoparticles is unlikely due to rapid H_2 desorption (at least in the case of UHV experiments). Concerning the formation of carbonaceous species, the lower barrier for CH dehydrogenation (21 kJ mol^{-1} as compared with Pt(111)) suggests easier carbon poisoning. It should be pointed out, however, that this effect is moderate, thus elevated temperatures should still be required for carbon formation. In agreement with these results, CH decomposition on stepped surfaces was observed in the temperature range 420–450 K.^[62]

Dehydrogenation of CH_4 on Pt nanoparticles supported on CeO_2 : Experiment:

To experimentally corroborate the theoretically predicted effect of particle edges and corner sites on methane activation and dehydrogenation, SSMB experiments were performed on the dissociation of methane on supported Pt nanoparticles. The reaction intermediates were detected in a time-resolved mode using HR-PES. As a model support, we used an ordered CeO_2 film prepared on Cu(111). The chemical and structural properties of the film were investigated previously.^[54,55,74] We have also investigated the growth of Pt nanoparticles on the film by means of scanning tunneling microscopy (STM).^[53] It was found that Pt grows in the form of three-dimensional islands with a nucleation density of around $5 \times 10^{12} \text{ cm}^{-2}$ under the conditions applied. Based on this value, it was estimated that the Pt nanoparticles contain, on average, around 600 Pt atoms, corresponding to an average particle size of around 3.3 nm.

In previous SSMB/XPS experiments using laboratory light sources, we have found the first indications that after initial methane activation and formation of CH_3 , dehydrogenation of these species proceeds spontaneously to CH and C, even at temperatures as low as 130 K.^[53] On the contrary, these reactions required significantly higher temperatures on both Pt(111)^[56] and on stepped Pt single-crystal surfaces.^[62,75] To further verify this observation, HR-PES experiments were performed by using synchrotron radiation, providing both better spectral and temporal resolution than what could be obtained in the previous experiments.

The development of the C 1s spectra upon continuous exposure of the Pt/ CeO_2 /Cu(111) sample to the SSMB of CH_4 at a sample temperature of 100 K is summarized in Figure 4a. To disentangle the contribution of any initial carbon contamination built up upon sample preparation, the C 1s spectra are represented as an intensity difference before and after exposure to methane. Several issues should be kept in mind at this point: first, it has been shown that high intensi-

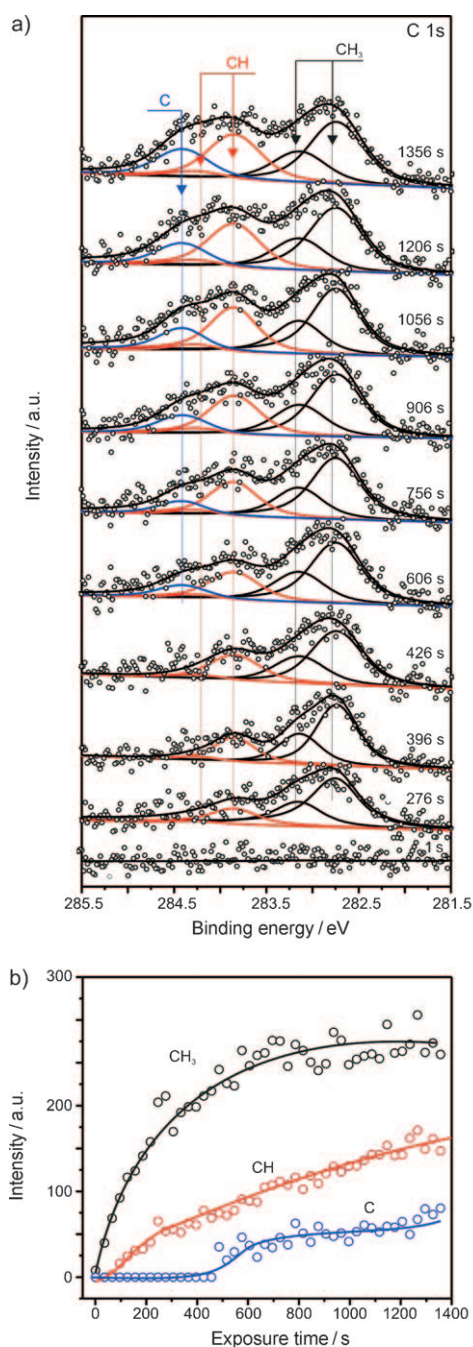


Figure 4. a) Development of C 1s spectra upon continuous exposure of the Pt/CeO₂/Cu(111) sample to the SSMB of CH₄ with a kinetic energy of 68 kJ mol⁻¹ (0.71 eV) at a sample temperature of 100 K. The spectra are represented as an intensity difference before and after exposure to CH₄. The peaks associated with CH₃, CH, and C are shown in black, red, and blue, respectively. b) Evolution of the species with an increasing time of exposure.

ty synchrotron radiation may rapidly induce surface reactions, including hydrocarbon dehydrogenation.^[56] We therefore minimized the acquisition time per spectrum to 5 s. Second, we have found that the spectral width of the com-

ponents is substantially larger than for comparable experiments on Pt single-crystal surfaces (compare with previous studies in the literature^[56,62,75]). This broadening is mainly due to two contributions: 1) a heterogeneity effect arising from the inequivalency of the adsorption sites on the Pt nanoparticles and 2) a final state effect arising from the intrinsic size distribution of the Pt nanoparticles. The latter is the result of the Coulomb energy on the nanoparticles in the photoemission final state and leads to a size-dependent binding energy (BE) shift.^[76] For size-distributed particles, this effect will result in a broadening of the PES signals with decreasing particle size.^[77]

The broadening effects make it difficult to directly identify the individual components in the experimental spectra. Therefore, the data has been fitted by using relative BE shifts and vibrational splittings from single-crystal experiments.^[56] A good description of the experimental spectra is obtained by assuming the presence of CH₃, CH, and C species on the Pt particles. At this point it is worth mentioning that, based on the DFT calculations, we could also consider a scenario in which methylene might be found as stable species on the nanoparticles (Figure 3). In fact, the energy barrier for CH₂ dehydrogenation is 25 kJ mol⁻¹ higher than that for methyl dehydrogenation. This difference suggests the possibility of the existence of a temperature regime at which methylene species are kinetically stable. On the basis of the present experimental data, however, we can neither identify CH₂, nor can we exclude completely the presence of such species. Therefore, and due to the lack of reference data on CH₂ on Pt single crystals, CH₂ species were not included in the present analysis.

The temporal evolution of the CH₃, CH, and C species is shown in Figure 4b. The initial product of methane activation is CH₃. In spite of the intrinsic broadening effects on particles, the vibrational fine structure is resolved. The corresponding adiabatic and first vibrationally excited components are located at 282.8 and 283.2 eV (Figure 4a, black lines). The binding energies of these components are in a good agreement with the experimental values for Pt(111).^[56] It is found that the intensity of CH₃ increases with CH₄ exposure before it saturates at an exposure time of approximately 900 s (≈ 90 L CH₄, 1 L = 10⁻⁶ torr s).

According to DFT results depicted in Figure 3, the activation barrier for the initial H abstraction of methane should be drastically reduced on specific sites of the Pt nanoparticles. In fact, activation barriers as low as 32 kJ mol⁻¹ can be found. Thus, the KE of 68 kJ mol⁻¹ used in the present experiment would be expected to be more than sufficient to efficiently overcome this first barrier. One has to keep in mind that this effect will be limited to direct dissociation events at very specific sites. The vast majority of sites on the particles will, however, be more similar to those on Pt(111). As a result, we expect to observe a superposition of dissociation events occurring at different types of sites with a broad distribution of barrier heights. Therefore, experimental verification of the reduced barrier height at minority sites will be experimentally demanding. It may, however, be

feasible to observe this effect by systematic studies of the KE dependence on the sticking coefficient using SSMBs with narrow KE distributions.

The primary information available from the present data concerns the further dehydrogenation steps leading to CH and C (Figure 4). The emergence of CH species is first detected in the spectra at an exposure time of around 66 s. CH was fitted as a vibrational split peak with an energy difference and intensity ratio adapted from Pt(111).^[56] The corresponding adiabatic and vibrationally excited components appear at 283.8 and 284.2 eV (Figure 4, red lines). Radiation-induced processes can be excluded at these low doses, suggesting that the activation barrier is overcome by thermal activation. The initially slow rate of CH formation suggests that CH is formed from CH₃ in a sequential reaction after thermalization. At higher CH₃ exposures (>200 L), the CH formation rate increases, resembling the dominant contribution of the CH species in C 1s spectra observed previously^[53] (note that CH₃ exposure for the period of 1400 s results in a total dose of about 140 L). This is in contrast with CH₃ formation, which saturates faster and most probably reflects a scenario in which a monolayer of methyl species is also formed at the interior of nanoparticle facets. A mass transfer of CH₃ moieties from the interior of the (111) facets to the edges can occur due to a low diffusion energy barrier, which is, according to our DFT estimation, 37 kJ mol⁻¹. This diffusion barrier can be sufficiently overcome at 100 K. No mass transfer is expected after the saturation coverage is reached.

It should be pointed out that the experimental findings are qualitatively consistent with previous XPS measurements and show that at slightly higher temperature (120 K) and on much longer timescales, the dehydrogenation of CH₃ and the formation of CH and C species occurs.^[53] As theoretically predicted, this behavior is in sharp contrast to CH₄ dehydrogenation on Pt single-crystal surfaces. On Pt(111), for example, CH₃ has been shown to remain stable up to 240 K.^[56] On stepped Pt(322) and Pt(355) surfaces, the onset temperature for CH₃ dehydrogenation was found to be reduced to around 200 and 150 K, respectively, suggesting a decrease of the activation barrier by about 20–40%.^[62] The observation of slow dehydrogenation on the Pt nanoparticles at around 100 K suggests that on the Pt nanoparticles the activation barrier for dehydrogenation is reduced drastically, even if compared to stepped surfaces. This finding is fully consistent with the DFT results, which predict a decrease in activation energy from 90 kJ mol⁻¹ on Pt(111) to 32 kJ mol⁻¹ for the most favorable sites on Pt₇₉ nanoparticles, that is, a decrease by about 65%. It is worthwhile noting that the effect of particle-specific sites on the activation barriers may be substantially larger than the effect of choosing different transition metals. For instance, a reduction of 15–30 kJ mol⁻¹ in the barrier height for the first methane dehydrogenation step was observed when changing from Ni(111) to Pt(111).^[32–35]

Finally, it should be noted that after extended reaction times, the very slow formation of atomic carbon was ob-

served. This is indicated by the appearance of a high BE shoulder in the CH peak at 284.4 eV (blue line in Figure 4). The low initial rate is in line with a sequential reaction, which suggests that C may be formed as the final product of dehydrogenation from CH. In principle, the formation of C is in line with the fact that the DFT calculations suggest that complete methane dehydrogenation represents the energetically most stable situation on Pt₇₉. The observation is somewhat surprising, since on Pt(111) methylidyne is stable up to around 450 K with no C formation observed^[56] at low temperature. On stepped Pt, CH dehydrogenation occurs at a lower temperature, around 350 K. The calculations predict a decrease in activation energy from 120 kJ mol⁻¹ on Pt(111) to 99 kJ mol⁻¹ on Pt₇₉ (see the reaction profile in Figure 3). This, however, cannot explain C formation at 100 K. Normally, a substantially higher reaction temperature would be expected.

At present, the origin of low-temperature CH decomposition is not completely understood. It must, however, be stressed that some effects remain untreated, yet limiting the comparability between experiment and theory. One main feature is that theoretical calculations are limited to low coverage, whereas the experiments have to be performed at larger coverage up to saturation. In the latter case, adsorbate–adsorbate interactions may drastically modify the energetics of the reaction pathway. In fact, upon saturation, steric repulsions among negatively charged CH species (see the section on DFT calculations) can increase the (CH+3H) energy level. Moreover, at saturation coverage, a graphitic phase of C can be formed, leading to a stabilization comparable with that of the carbidic C phase.^[46] In addition, at longer exposure times the accumulation of beam damage cannot be completely ruled out, which could also contribute to the favoring of CH dehydrogenation to carbon. Finally, other effects that have not been accounted for, such as the influence of sites at the metal oxide boundary or the presence of very small Pt aggregates, might also contribute to an easier C formation.

Conclusion

Methane activation and dehydrogenation was studied by state-of-the-art DFT methods on nanoparticle and Pt(111) single-crystal models. The theoretical results were compared to experimental data on supported Pt model catalysts obtained by a SSMB methods and HR-PES.

DFT calculations show that CH₃ and CH₂ intermediates are remarkably stabilized at sites located at particle edges and corners by 50–80 kJ mol⁻¹. The stabilization of other species, namely, CH₄, CH, C, and H, also occurs, although to a lesser extent. This general stabilization seems to have its origin in a combination of two contributions: low-coordinated sites are, on the one hand, more active to bind species and, on the other hand, exhibit a larger flexibility to accommodate the adsorbates. Such effects are translated into substantial differences in thermodynamics and kinetics for the

dehydrogenation reaction energy profile of methane when comparing extended Pt(111) surfaces with Pt nanoparticles.

Methyl and methylene formation reaction steps are endothermic on Pt(111), whereas they are markedly exothermic on Pt₇₉. The change in exothermicity is also reflected by a strong decrease of the activation barriers for the corresponding reaction steps. The activation barrier for the first methane C–H scission, which is normally the rate-limiting step, is reduced on Pt₇₉ by approximately 60 kJ mol⁻¹, whereas the energy barrier for methylene formation is reduced by around 40 kJ mol⁻¹. Furthermore, DFT results suggest that CH₂ may be a stable intermediate on Pt nanoparticles within a narrow temperature range. Another implication of the usage of Pt nanoparticles is that C instead of CH represents the thermodynamically most favorable state, potentially accelerating carbon accumulation.

Methane activation and dehydrogenation has been experimentally investigated on Pt nanoparticles supported on an ordered CeO₂ film on Cu(111). A high KE-SSMB was applied to activate methane, with the reaction products being detected in a time-resolved mode by synchrotron-based HRPES. In accordance with the theoretical results, it was shown that dehydrogenation is much more facile on Pt nanoparticles, both in comparison to the Pt(111) single crystal and to stepped Pt surfaces. Specifically, it was observed that CH₃ generated on the Pt nanoparticles in a direct dissociation process undergoes spontaneous, thermally induced dehydrogenation, even at surface temperatures as low as 100 K.

In summary, a pronounced effect of specific Pt nanoparticle sites on methane-activation-related reactions is observed. It has been shown to be related to the presence of edge, corner, and nearby sites, which bind reaction intermediates CH_x more strongly. This effect makes methane activation a downhill process and strongly reduces the activation barriers. It should be noted that this nanoparticle effect is more important than the differences observed for different active metals, for example, comparing extended (111) surfaces of Ni and Pt. Present results are related to the initial steps of the steam reforming and coupling of CH₄ with CO₂. The current work provides general insights into methane activation processes.

Acknowledgements

F.V. thanks the Alexander von Humboldt Foundation for financing his postdoctoral grant. F.V. and A.G. gratefully acknowledge computational time provided by the Regionales Rechenzentrum Erlangen. Participation of K.N. has been supported by the Spanish MICINN (grants FIS2008-02238, HA2006-0102 and ERACHEM project No. CTQ2007-30547-E/BQU). The authors also acknowledge financial support by the Deutsche Forschungsgemeinschaft (DFG) within the ERACHEM program (“NanoFunC” project), additional support from the DFG within the Excellence Cluster “Engineering of Advanced Materials” (<http://www.eam.uni-erlangen.de>) in the framework of the excellence initiative and COST-D41 Action. Y.L., T.S. and M.P.A.L. thank the Helmholtz Zentrum Berlin at BESSY II for financial support and the staff of BESSY II for the prompt assistance during the beamtime. The authors thank Prof. V.

Matolín (Charles University, Prague) for advising on the preparation of CeO₂ films on Cu(111).

- [1] J. Feichter, U. Schurath, R. Zellner, *Chem. Unserer Zeit* **2007**, *41*, 138.
- [2] P. M. Tornaiainen, X. Chu, L. D. Schmidt, *J. Catal.* **1994**, *146*, 1.
- [3] J. Wei, E. Iglesia, *J. Catal.* **2004**, *224*, 370.
- [4] F. Besenbacher, I. Chorkendoff, B. S. Clausen, B. Hammer, A. M. Molenbroek, J. K. Nørskov, I. Stensgaard, *Science* **1998**, *279*, 1913.
- [5] J. P. Van Hook, *Catal. Rev. Sci. Eng.* **1980**, *21*, 1.
- [6] G. F. Froment, *J. Mol. Catal. A* **2000**, *163*, 147.
- [7] M. C. Bradford, M. A. Vannice, *Catal. Rev. Sci. Eng.* **1999**, *41*, 1.
- [8] Y. H. Hu, E. Ruckenstein, *Adv. Catal.* **2004**, *48*, 297.
- [9] A. T. Ashcroft, A. K. Cheetham, M. L. H. Green, P. D. F. Vernon, *Nature* **1991**, *352*, 225.
- [10] M. C. J. Bradford, M. A. Vannice, *Appl. Catal. A* **1996**, *142*, 97.
- [11] K. Tomishige, Y.-G. Chen, K. Fujimoto, *J. Catal.* **1999**, *181*, 91.
- [12] Z. L. Zhang, X. E. Verykios, *Catal. Today* **1994**, *21*, 589.
- [13] M. Pettre, C. Eichner, M. Perrin, *J. Chem. Soc. Faraday Trans.* **1946**, *43*, 335.
- [14] D. Dissanyake, M. P. Rosynek, K. C. C. Kharas, J. H. Lunsford, *J. Catal.* **1991**, *132*, 117.
- [15] D. A. Hickman, L. D. Schmidt, *Science* **1993**, *259*, 343.
- [16] V. R. Choudhary, A. M. Rajput, B. Prabhakar, *J. Catal.* **1993**, *139*, 326.
- [17] B. E. Bent, *Chem. Rev.* **1996**, *96*, 1361.
- [18] W. A. Herrmann, *Angew. Chem.* **1982**, *94*, 118; *Angew. Chem. Int. Ed. Engl.* **1982**, *21*, 117.
- [19] P. Biloen, W. M. H. Sachtler, *Adv. Catal.* **1981**, *30*, 165.
- [20] V. F. Fischer, H. Tropsch, *Brennst.-Chem.* **1928**, *3*, 39.
- [21] T. V. Choudhary, C. Sivadinarayana, C. C. Chusuei, A. Klinghoffer, D. W. Goodman, *J. Catal.* **2001**, *199*, 9.
- [22] M. G. Poirier, C. Sapundzhiev, *Int. J. Hydrogen Energy* **1997**, *22*, 429.
- [23] E. K. Lee, S. Y. Lee, G. Y. Han, B. K. Lee, T.-J. Lee, J. H. Jun, K. J. Yoon, *Carbon* **2004**, *42*, 2641.
- [24] G. E. Keller, M. M. Bhasin, *J. Catal.* **1982**, *73*, 9.
- [25] P. D. F. Vernon, M. L. H. Green, A. K. Cheetham, A. T. Ashcroft, *Catal. Today* **1992**, *13*, 417.
- [26] M. Mleczko, M. Bearns, *Fuel Process. Technol.* **1995**, *42*, 217.
- [27] J. H. Lunsford, *Angew. Chem.* **1995**, *107*, 1059; *Angew. Chem. Int. Ed. Engl.* **1995**, *34*, 970.
- [28] R. D. Beck, P. Maroni, D. C. Papageorgopoulos, T. T. Dang, M. P. Schmid, T. R. Rizzo, *Science* **2003**, *302*, 98.
- [29] A. C. Luntz, *Science* **2003**, *302*, 70.
- [30] R. R. Smith, D. R. Killelea, D. F. DelSesto, A. L. Utz, *Science* **2004**, *304*, 992.
- [31] S. G. Wang, X. Y. Liao, J. Hu, D. B. Cao, Y. W. Li, J. Wang, H. Jiao, *Surf. Sci.* **2007**, *601*, 1271.
- [32] M.-S. Liao, C.-T. Au, C.-F. Ng, *Chem. Phys. Lett.* **1997**, *272*, 445.
- [33] S. Nave, B. Jackson, *J. Chem. Phys.* **2009**, *130*, 054701.
- [34] A. B. Anderson, J. J. Maloney, *J. Phys. Chem.* **1988**, *92*, 809.
- [35] R. Bisson, M. Sacchi, T. T. Dang, B. Yoder, P. Maroni, R. D. Beck, *J. Phys. Chem. A* **2007**, *111*, 12679.
- [36] A. Michaelides, P. Hu, *J. Chem. Phys.* **2001**, *114*, 2523.
- [37] A. Michaelides, P. Hu, *J. Chem. Phys.* **2001**, *114*, 5792.
- [38] D. C. Ford, Y. Xu, M. Mavrikakis, *Surf. Sci.* **2005**, *587*, 159.
- [39] M. A. Petersen, S. J. Jenkins, D. A. King, *J. Phys. Chem. B* **2004**, *108*, 5920.
- [40] G. Psafogiannakis, A. St-Amant, M. Ternan, *J. Phys. Chem. B* **2006**, *110*, 24593.
- [41] J. Kua, W. A. Goddard III, *J. Am. Chem. Soc.* **1999**, *121*, 10928.
- [42] J. Kua, W. A. Goddard III, *J. Phys. Chem. B* **1998**, *102*, 9492.
- [43] G. Kresse, J. Furthmüller, *Phys. Rev. B* **1996**, *54*, 11169.
- [44] P. E. Blöchl, *Phys. Rev. B* **1994**, *50*, 17953.
- [45] B. Hammer, L. B. Hansen, J. K. Nørskov, *Phys. Rev. B* **1999**, *59*, 7413.

- [46] F. Viñes, K. M. Neyman, A. Görling, *J. Phys. Chem. A* **2009**, *113*, 11963.
- [47] F. Viñes, A. Desikumastuti, T. Staudt, A. Görling, J. Libuda, K. M. Neyman, *J. Phys. Chem. C* **2008**, *112*, 16539.
- [48] F. Viñes, C. Löschen, F. Illas, K. M. Neyman, *J. Catal.* **2009**, *266*, 59.
- [49] I. V. Yudanov, R. Sahnoun, K. M. Neyman, N. Rösch, *J. Chem. Phys.* **2002**, *117*, 9887.
- [50] F. Viñes, F. Illas, K. M. Neyman, *Angew. Chem.* **2007**, *119*, 7224; *Angew. Chem. Int. Ed.* **2007**, *46*, 7094.
- [51] A. Roldán, F. Viñes, F. Illas, J. M. Ricart, K. M. Neyman, *Theor. Chem. Acc.* **2008**, *120*, 565.
- [52] F. Viñes, F. Illas, K. M. Neyman, *J. Phys. Chem. A* **2008**, *112*, 8911.
- [53] Y. Lykhach, T. Staudt, M. P. A. Lorenz, R. Streber, A. Bayer, H.-P. Steinrück, J. Libuda, *ChemPhysChem.* **2010**, DOI: 10.1002/cphc.200900673.
- [54] F. Sutara, M. Cabala, L. Sedlacek, T. Skala, M. Skoda, V. Matolín, K. C. Prince, V. Chab, *Thin Solid Films* **2008**, *516*, 6120.
- [55] V. Matolín, J. Libra, I. Matolinova, V. Nehasil, L. Sedlacek, F. Sutara, *Appl. Surf. Sci.* **2007**, *254*, 153.
- [56] T. Fuhrmann, M. Kinne, B. Tränkenschuh, C. Papp, J. F. Zhu, R. Denecke, H.-P. Steinrück, *New J. Phys.* **2005**, *7*, 107.
- [57] R. S. Vincent, R. P. Lindstedt, N. A. Malik, I. A. B. Reid, B. E. Messenger, *J. Catal.* **2008**, *260*, 37.
- [58] T. Jacob, W. A. Goddard III, *J. Phys. Chem. B* **2005**, *109*, 297.
- [59] J. P. Perdew, Y. Wang, *Phys. Rev. B* **1992**, *45*, 13244.
- [60] E. Shustorovich, H. Sellers, *Surf. Sci. Rep.* **1998**, *31*, 1.
- [61] R. F. W. Bader, R. J. Gillespie, P. J. MacDougall, *J. Am. Chem. Soc.* **1988**, *110*, 7329.
- [62] C. Papp, B. Tränkenschuh, R. Streber, T. Fuhrmann, R. Denecke, H.-P. Steinrück, *J. Phys. Chem. C* **2007**, *111*, 2177.
- [63] I. V. Yudanov, A. V. Matveev, K. M. Neyman, N. Rösch, *J. Am. Chem. Soc.* **2008**, *130*, 9342.
- [64] A. P. Graham, A. Menzel, J. P. Toennies, *J. Chem. Phys.* **1999**, *111*, 1676.
- [65] J. Harris, J. Simon, A. C. Luntz, B. Mullins, T. Rettner, *Phys. Rev. Lett.* **1991**, *67*, 652.
- [66] C. T. Campbell, Y.-K. Sun, W. H. Weinberg, *Chem. Phys. Lett.* **1991**, *179*, 53.
- [67] J. Wei, E. Iglesia, *J. Phys. Chem. B* **2004**, *108*, 4094.
- [68] C. J. Cramer, D. G. Truhlar, *Phys. Chem. Chem. Phys.* **2009**, *11*, 10757.
- [69] M.-S. Liao, C.-T. Au, C.-F. Ng, *Chem. Phys. Lett.* **1997**, *272*, 445.
- [70] A. D. Becke, *J. Chem. Phys.* **1993**, *98*, 5648.
- [71] A. Michaelides, P. Hu, *J. Am. Chem. Soc.* **2000**, *122*, 9866.
- [72] J. P. Perdew, K. Burke, M. Ernzerhof, *Phys. Rev. Lett.* **1996**, *77*, 3865.
- [73] H. Ueta, M. Saida, C. Nakai, Y. Yamada, M. Sasaki, S. Yamamoto, *Surf. Sci.* **2004**, *560*, 183.
- [74] T. Staudt, Y. Lykhach, L. Hammer, M. A. Schneider, V. Matolín, J. Libuda, *Surf. Sci.* **2009**, *603*, 3382.
- [75] C. Papp, T. Fuhrmann, B. Tränkenschuh, R. Denecke, H.-P. Steinrück, *Chem. Phys. Lett.* **2007**, *442*, 176.
- [76] G. K. Wertheim, S. B. DiCenzo, D. N. E. Buchanan, *Phys. Rev. B* **1986**, *33*, 5384.
- [77] M. Bäumer, H.-J. Freund, *Prog. Surf. Sci.* **1999**, *61*, 127.

Received: February 3, 2010
Published online: April 23, 2010